Journal of Applied Polymer Science

Self-Assembly of Poly(3-hexyl thiophene)-*b*-Poly(ethylene oxide) into Cylindrical Micelles in Binary Solvent Mixtures

Jingyi Li,[1]* Xian Li,[2]* Debin Ni,[2] Jianying Wang,[1] Guoli Tu,[2] Jintao Zhu[1]

[1]Key Laboratory for Large-Format Materials and Systems of the Ministry of Education, School of Chemistry and Chemical Engineering, Huazhong University of Science and Technology (HUST), Wuhan 430074, People's Republic of China

*These authors contribute equally to this work.

[2]Wuhan National Laboratory of Optoelectronics, HUST, Wuhan 430074, China

Correspondence to: J. Zhu (E-mail: jtzhu@mail.hust.edu.cn) and G. Tu (E-mail: tgl@mail.hust.edu.cn)

ABSTRACT: Asymmetric block copolymer based on regioregular poly(3-hexyl thiophene) (P3HT) and poly(ethylene oxide) (PEO) was synthesized through Heck reactions. The addition of PEO block has no influence in the effective conjugation length of P3HT block and apparently provides colloidal stability for the formation of stable nanostructures. Introduction of poor solvent to good solvent containing P3HT-*b*-PEO will induce the crystallization-driven assembly of the P3HT into cylindrical micelles with a P3HT core, owing to π–π stacking of the conjugated backbone of P3HT. The absorption spectra of the cylindrical micelles reveal a red shift as compared to the polymer in good solvent, indicating the extension of conjugation length with an improved π–π stacking of the polymer chains within the cylindrical micelles. Our results indicated that cylindrical micelles with varied diameter and length can be obtained when solvent properties were varied using several different binary solvent mixtures. More interestingly, we demonstrate that ultrasonic processing can fragment the cylindrical micelles only when the ratio of poor solvent increases. This provides a facile and effective way to fabricate cylindrical micelles for applications in the area of polymer solar cell as well as organic optoelectronics device. © 2014 Wiley Periodicals, Inc. J. Appl. Polym. Sci. **2014**, *131*, 41186.

KEYWORDS: copolymers; micelles; nanoparticles; nanowires and crystals; self-assembly

Received 3 April 2014; accepted 18 June 2014

DOI: 10.1002/app.41186

INTRODUCTION

Conjugated polymers are widely studied as an alternative to inorganic single-crystalline semiconductors in the area of optoelectronic devices due to their advantages, including low cost, light weight, flexibility, and the ability of large-area fabrication.[1–10] Block copolymers (BCPs) containing polythiophene (PT) become more and more attractive because of its high hole mobility and favorable processability for optoelectronic device applications, such as photovoltaics (PV)[11–16] and organic field-effect transistor (OFET).[17–19] Although PT-based BCPs are widely investigated and the referring researches are ever-increasing, their applications are still limited due to the poor performance, primarily originating from the poor solution processability.

It has been demonstrated that the precision structure on the nanometer/micrometer scales plays a key role in determining the properties and ultimate device performance, besides the intrinsic photoconductivity of the conducting polymers.[8,20–24] One dimensional (1D) nanostructures of conjugated polymers (nanofibers or cylindrical micelles), where chains are modified by the increased interchain stacking resulting from π–π interactions, offer the possibility that directs charge transport and further improves efficiency of PV or OFET due to better chains ordering.[25–27] The regiospecific placement of the alkyl substituents in regioregular poly(3-hexyl thiophene) (P3HT) promotes self-assembly of the polymer into densely packed, elongated nanofibers of uniform width. During the past decades, PT-contained nanofibers were generally produced via thin film deposition method,[16,28–31] electrospinning (ES),[32–34] or solution processing approach.[35–38] However, for the film formation process, the morphologies produced by typical spin-coating method are kinetically trapped due to the fast evaporation of the solvent. Postprocessing, including thermal or solvent annealing, is usually needed to trigger the formation of cylindrical domains as well as improved charge mobility. Meanwhile, the nanofibers made from ES are usually hundreds of nanometers, seldom reaching several nanometers in diameter. Nowadays, P3HT homopolymer is found to self-organize into nanofibers in solution when varying the properties of the solvent from a favorable

to unfavorable media owing to the crystallization of the backbone,[39,40] but systems based on this strategy are often hampered by the poor solubility/colloidal stability and unfavorable fibers aggregation. On the other hand, BCPs are a versatile class of materials that have the ability to self-assemble at the nanoscale.[41–43] In this fashion, significant advances have been made toward limiting aggregation and controlling the assembly structures of BCPs containing conjugated polymer, triggering the formation of spherical micelles, cylindrical micelles, and helical structures.[24,35] The rod-coil BCPs containing conjugated core-forming block, which simultaneously have the rigidity of thiophene rings and the controllability of flexible chains, provide more flexibility for tuning the structures of the aggregates compared to the P3HT homopolymer.[28,35] The formed structures are more thermodynamically stable than those created by polymer blends. Moreover, the scale of these structures lies in the order of tens nanometer, which allows photo-generated excitons to reach the interface between *p*- and *n*-type semiconductors effectively.[44] Thus, it is desirable to develop facile solution self-assembly strategies for the formation of cylindrical micelles based on rod-coil BCPs containing highly crystalline conjugated block as their inherent crystallinity may significantly improve device performance.[16,17]

We are particularly interested in generating BCP cylindrical micelles through the solution self-assembly route from which well-defined nanostructures can be generated.[45,46] Generally, phase behavior of thiophene-contained BCPs is much different from conventional BCPs with all noncrystalline chains because crystallization of the rod block gives rise to additional driving force for the microphase separation. Previous studies demonstrated that cylindrical micelles produced from assembly of conjugated BCPs in solution are highly crystalline[40,47–49] and promise improvement over conventional thin-film processing in organic PV devices is achieved. Importantly, BCPs with the fine-tuned self-assembly structure of molecular design and processing can enhance the effectiveness of internal processes, including charge transporting characteristics, field-effect mobility, spectrum, and efficiency of emission in LEDs, charge separation process in photodiodes, and environmental stability, ultimately improving the performance of optoelectronic devices.[17,48,50] However, the self-assembly of such polymers into crystalline nanostructures with precisely controlled widths and lengths has seldom been reported.[35,36] In addition, few efforts have been paid on the systematic investigation of solvent properties effect on the self-assembly behaviors of BCPs with conjugated blocks.

Herein, we report the synthesis of amphiphilic regioregular P3HT and poly(ethylene oxide) (PEO) BCPs with a low polydispersity index (PDI = 1.23) through the Heck reactions. PEO block was chosen due to its good solubility in a series of solvents, including water and commonly used polar organic solvents. It has been proved that, with the addition of PEO block, the solubility of the copolymer in solution improved greatly and had little influence on its crystallinity of P3HT.[37] Owing to the amphiphilic nature of the formed BCPs, P3HT-*b*-PEO can self-assemble into well-defined cylindrical micelles with tunable diameter and length by using a series of good/poor solvent mixtures. Furthermore, we show that ultrasonic processing can fragment the cylindrical micelles while keeping the diameter unchanged. Our study indicates that self-assembly of P3HT-*b*-PEO in mixed solvents provides a facile and versatile way to fabricate cylindrical micelles with a certain width and length, potentially useful in optoelectronics device.

EXPERIMENTAL

Materials

All reagents and solvents were purchased from Sinopharm Chemical Reagent and used without further purification unless noted. Poly(ethylene oxide) (PEO, PDI = 1.08), was purchased from Polymer Source.

Sample Preparation

Synthesis of Poly(3-hexylthiphene). 2-bromo-3-hexylthiphene (7.4 g, 30 mmol) was dissolved in THF under nitrogen. Then, lithium diisopropylamide (LDA) (2 mol mL^{-1}, 15 mL) was injected at −78°C. After stirring for an hour, anhydrous $ZnCl_2$ (5 g, 36 mmol) was added to the above system; after stirring for another hour, the system was warmed to room temperature and $Ni(dppp)Cl_2$ (0.2 g, 0.37 mmol) was then added. After reacting for 20 min, the mixture was precipitated in 400 mL of methanol, and the precipitates were extracted on Soxhlet apparatus with methanol, acetic ether, *n*-hexane, DCM, and chloroform. The chloroform fraction was collected after removing solvent under reduced pressure. Yield: 20.3%, $M_n = 9340$, $M_w/M_n = 1.18$.

Terminal Modification of PEO by Benzoic Acid (PEO-EBA). PEO (5 g, 1 mmol), 4-ethynyl benzoic acid (330 mg, 1.8 mmol) were dissolved in CH_2Cl_2 (DCM, 15 mL).Then, *N*, *N*′-dicyclohexylcarbodiimide (DCC) (2 g, 9.7 mmol) and 4-(dimethylamino) pyridine (DMAP) (0.2 g, 1.6 mmol) dissolved in CH_2Cl_2 (15 mL) were added dropwise at room temperature. After overnight stirring, the sample was washed by 10 wt % NaOH (2 × 50 mL) and brine (2 × 100 mL), and then precipitated in 500 mL of diethyl ether. The precipitates were washed with diethyl ether for several times and dried in vacuum (3.8 g, 74.1%).

Synthesis of P3HT-*b*-PEO. $Pd(OAc)_2$ (7 mg, 0.03 mmol), PPh_3 (15.8 mg, 0.06 mmol), CuI (5.7 mg, 0.03 mmol), Et_3N (3 mL), P3HT ($M_n = 9340$, 250 mg), and PEO-EBA ($M_n = 5129$, 3.3 g) were added to a two-neck flask. Then, anaerobic THF (30 mL) was injected into the flask under nitrogen. After the system was stirring at 60°C for 3 days, the mixture extracted by $CHCl_3$ (100 mL) was washed with brine (3 × 100 mL) and then dried by anhydrous sodium sulfate. After filtering, the sample was concentrated by rotary evaporation, and then precipitated in methanol. The collected precipitates were extracted on Soxhlet apparatus with methanol and DCM. Yield: 32.3%, $M_n = 14{,}880$, $M_w/M_n = 1.23$, ^1H NMR (400 MHz, $CDCl_3$, δ): 6.97 (s, 1H), 3.64 (s, 8H,), 2.80 (b, 2H), 1.70 (b, 2H), 1.35–1.43 (m, 6H), 0.91 (b, 3H).

Preparation of P3HT-*b*-PEO Cylindrical Micelles. In a typical experiment, P3HT-*b*-PEO was first dissolved in toluene at a concentration of 0.25 mg mL^{-1} at room temperature. The solution was then kept stirring overnight to guarantee that the

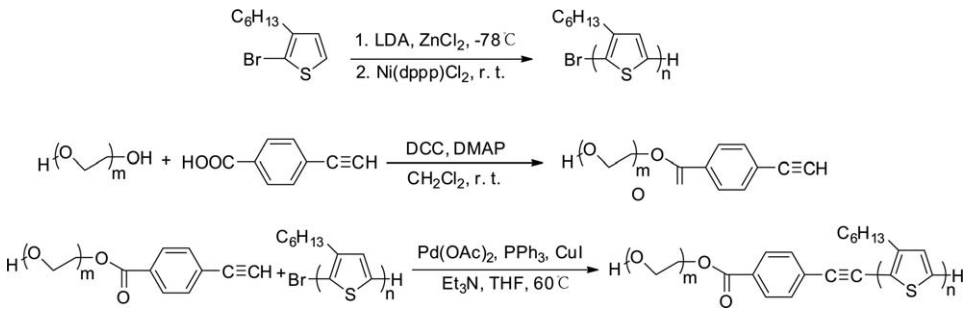

Scheme 1. Synthesis procedure of P3HT-*b*-PEO.

copolymer was dissolved completely, yielding a clear orange solution. Et_2O was then added to the solution with a syringe pump with the speed of 200 μL min^{-1} under mild stirring until the volume ratio of toluene to Et_2O was 1 : 1. The resulting solution was then sealed and standing in dark and vibrationless environment over 2 days at room temperature to obtain homogeneous solution. A series of solutions with different volume ratio of Et_2O to toluene from 0.5 : 1 to 4 : 1 were prepared in a similar fashion. In ultrasonic processing experiments, the working frequency of ultrasonication is kept at 40 KHz. P3HT-*b*-PEO solutions were oscillated for 10 min at temperature of 25°C with oscillating power of 100%.

Characterization

Gel permeation chromatography (GPC, pl-gpc 50, Polymer Laboratories, A Varian) was performed by using THF as eluent and PS as standard sample. The column temperature was 40°C and the flow was 1 mL min^{-1}. ^1H NMR spectra of the polymer solutions in $CDCl_3$ were collected on a Bruker Avance 400 MHz spectrometer. Transmission electron microscopy (TEM) investigation was carried out using Tecnai G2 20 TEM (FEI) at an accelerated voltage of 200 kV. A drop of cylindrical micelles suspension was placed on copper grids precoated with a carbon thin film and dried completely at room temperature. Scanning electron microscopy (SEM) measurement was carried out using Sirion 200 SEM (FEI) at an accelerated voltage of 10 kV. A drop of cylindrical micelles suspension was placed on silicon wafer and dried completely at room temperature. Silicon wafers were treated with piranha solution (3 : 1 v/v 98% H_2SO_4: 30% H_2O_2) for half an hour at 70°C, sonicated in large amounts of deionized water for several times, rinsed with ethanol, and dried in a steam of nitrogen (caution: piranha solution is very corrosive and can react violently with organics, so careful measures should be taken). Atomic force microscopy (AFM) images were measured by the AFM (Veeco dimension 3100) using tapping mode. A phosphorus (*n*) doped silicon probe (Veeco, RTESP) with a resonant frequency around 370 kHz was used in this experiment. Silicon wafers were treated the same as mentioned above. Thin film of P3HT-*b*-PEO cylindrical micelles was spin coated from the solution onto silicon wafer at speed of 1000 rpm for 30 s. UV–vis absorption spectra were recorded using a UV–vis spectrophotometer (Rayleigh UV-1801). P3HT-*b*-PEO solution was placed in a 1-mm-thick quartz cell before measurement. X-ray diffraction (XRD) patterns were obtained on a PANalytical B.V. Instrument (X'Pert PRO). The X-ray profile was recorded from 5° to 30° with a 0.01° step size. Cylindrical micelles powders were prepared for XRD by centrifuging for 30 min at 5000 rpm twice and collecting after drying in vacuum oven.

RESULTS AND DISCUSSION

Syntheses of P3HT-*b*-PEO

$P3HT_{9k}$-*b*-PEO_{5k} diblock copolymer was synthesized following the procedure of previous report (see Scheme 1).[51–53] The P3HT block was prepared by GRIM polymerization (using $Ni(dppp)Cl_2$) to give P3HT with a living chain-end, which was chain extended into the diblock structure using the terminal modification of PEO by 4-ethynyl benzoic acid. The polystyrene-equivalent molecular weights estimated by GPC using THF as the eluent are shown in Table I. The actual ratio of the block lengths was determined by ^1H NMR spectroscopy (see Figure 1).

Self-Assembly of P3HT-*b*-PEO in Mixed Solvents

Due to the appearance of PEO segment, the P3HT-*b*-PEO can be dissolved in many conventional organic solvents at room temperature such as chloroform, toluene and THF. Here, we used toluene as good solvent, and added poor solvent Et_2O to induce the aggregation of P3HT-*b*-PEO. The introduction of Et_2O was accompanied by a marked color change from orange to dark red, which is commonly associated with the formation of crystalline P3HT aggregates in solution.[38] Figure 2(a) shows the UV–vis absorption spectra of P3HT-*b*-PEO in Et_2O/toluene system with different volume ratio. In toluene, where both polymer blocks are soluble, the spectrum shows a single absorption peak at 450 nm, which is the characteristic peak of P3HT homopolymer in good solvents which can be assigned to the intrachain π–π^* transition.[54] This observation indicates that the

Table I. Characteristics of the P3HT-*b*-PEO, Parent P3HT and PEO Homopolymers

Polymer	M_n (g mol^{-1})	M_w (g mol^{-1})	M_w/M_n
P3HT[a]	9340	11,064	1.18
PEO[b]	5000	5400	1.08
P3HT-PEO[a]	14,880	18,320	1.23

[a] Determined by GPC.
[b] Provided by Polymer Source. Mass fraction of P3HT in the copolymer is 0.63.

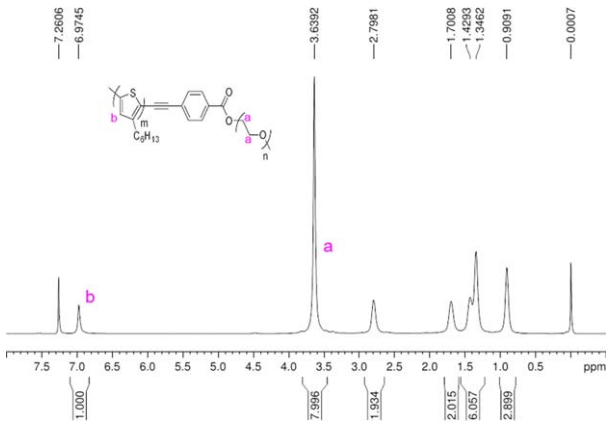

Figure 1. ^{1}H NMR spectrum of P3HT-*b*-PEO in $CDCl_3$. The asterisk denotes residual solvent signal. The signals in the range of 0.91–2.80 ppm are for hexyl protons. [Color figure can be viewed in the online issue, which is available at wileyonlinelibrary.com.]

incorporation of PEO segment does not decrease the effective conjugation length of P3HT block.

To figure out role of solution solubility in the formation of cylindrical micelles, different amount of poor solvent was introduced to the polymer solution. With the increase of volume ratio of Et_2O/toluene from 0.5 : 1 to 3 : 1, gradual red shift of UV–vis absorption maximum λ_{max} is observed, which is indicative of the increased planarity of the packed P3HT-*b*-PEO chains in the assemblies.[36,39,55] Addition of poor solvent to the solution leads to a bathochromic shift of π–π^* absorption band following the appearance of two more vibronic or "shoulder" peaks at 550 and 600 nm, and the vibration intensity (reflect in peaks at 550 and 600 nm) is much more intense. Those shoulder peaks are associated with crystalline order and results from an improved intermolecular interaction (π–π stacking) of the regioregular P3HT chains within the nanofibers.[55–58] Recent reports indicate a lamellar organization of polymer chains with π–π stacking along the extended polymer backbone direction.[59–61] Figure 2(b) shows a powder XRD spectrum from cylindrical micelles solutions formed in Et_2O/toluene at 2 : 1, exhibiting a peak at $2\theta = 5.4°$ for the (100) reflection which is characteristic of the interchain distance for interdigitated alkyl chains in P3HT ($d = 1.61$ nm). The signal at $2\theta = 23.2°$ ($d = 0.38$ nm) corresponding to the (010) reflection is attributed to the stacking distance of successive thiophene rings between two polymer chains, suggesting a crystalline self-organized lamellar morphology with 3D ordering of the regioregular P3HT polymer chains. The XRD data fits well with the UV–vis absorption spectra and the model. Generally, solubility parameter (δ) of PEO ($\delta_{PEO} = 17.7$ MPa$^{1/2}$) is more close to that of Et_2O ($\delta_{Et2O} = 7.4$ MPa$^{1/2}$) compared to that of P3HT ($\delta_{P3HT} = 20.0$ MPa$^{1/2}$),[62–64] indicating that the solubility of PEO is better than that of P3HT in Et_2O. Thus, with the addition of poor solvent Et_2O, P3HT will aggregate first to form the core of the cylindrical micelles while PEO will form the shell of the micelles. Figure 2(c) represents the schematic illustration of the cylindrical micelles formed from the self-assembly of P3HT-*b*-PEO in binary mixed solvents, according to the above results.

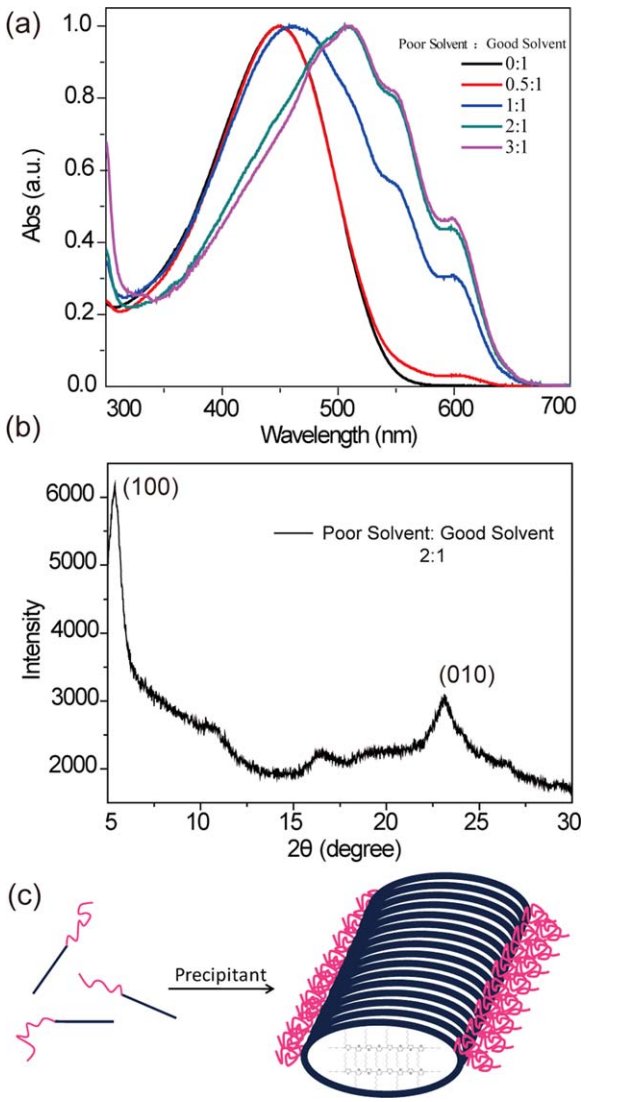

Figure 2. (a) UV–vis spectra of P3HT-*b*-PEO (0.25 mg mL^{-1}) in Et_2O/toluene at different ratio. With the increase of Et_2O, the λ_{max} has red shifted from 450 to 520 nm, and there appears two more vibronic or "shoulder" peaks at 550 and 600 nm. (b) Powder XRD spectra from cylindrical micelles solutions formed in Et_2O/toluene at 2 : 1. (c) Schematic illustration of the cylindrical micelles formation from the self-assembly of amphiphilic P3HT-*b*-PEO in mixed solvents; crystallization of P3HT induces the assembly of the BCPs in the solution. [Color figure can be viewed in the online issue, which is available at wileyonlinelibrary.com.]

Figure 3 shows the TEM images of cylindrical micelles formed from self-assembly of P3HT-*b*-PEO in Et_2O/toluene mixture with increasing the volume ratio of Et_2O/toluene from 0.5 : 1 to 3 : 1. According to the images, the widths of the cylindrical micelles are calculated to be 10.75 ± 2.09, 12.72 ± 2.33, 10.09 ± 1.51, and 8.43 ± 1.31 nm for Et_2O/toluene of 0.5 : 1, 1 : 1, 2 : 1, and 3 : 1, respectively. Notably, no staining of the samples was necessary to obtain sufficient contrast for the bright field TEM images, presumably as a result of efficient π packing of P3HT chains in the core involving stacking of the thiophene rings. Figure 4 shows the AFM and SEM images of the

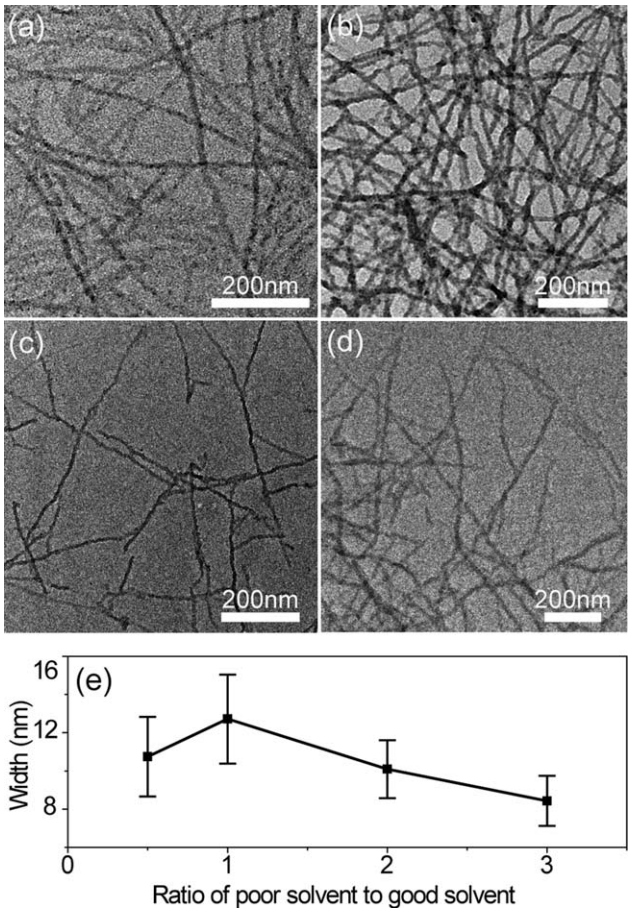

Figure 3. TEM images of the cylindrical micelles formed from self-assembly of P3HT-*b*-PEO in Et_2O/toluene with different ratio: (a) 0.5 : 1, (b) 1 : 1, (c) 2 : 1, (d) 3 : 1. (f) Relationship between the Et_2O/toluene ratio and the diameter of the cylindrical micelles. The diameters were measured by using Image J software and 500 cylindrical micelles were counted. Error bars represent the standard deviation.

cylindrical micelles obtained from Et_2O : toluene = 3 : 1. Clearly, cylindrical micelles with diameter of 8.98 ± 1.60 nm and length of greater than 1 μm were obtained in our study. Besides the widths, the UV–vis spectra show different curves, which may result from the varied solubility of the polymer in the solution. With the Et_2O drops into the copolymer solution,

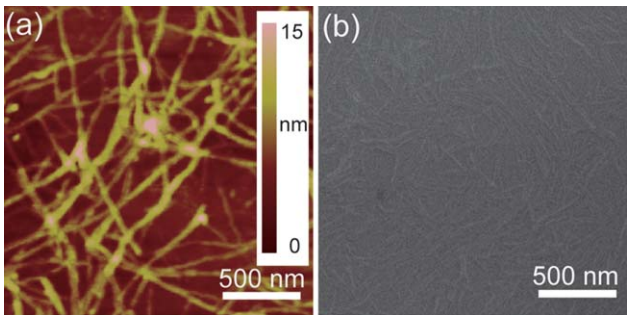

Figure 4. (a) AFM and (b) SEM images of the cylindrical micelles formed from self-assembly of P3HT-*b*-PEO in Et_2O/toluene with ratio of 3 : 1. [Color figure can be viewed in the online issue, which is available at wileyonlinelibrary.com.]

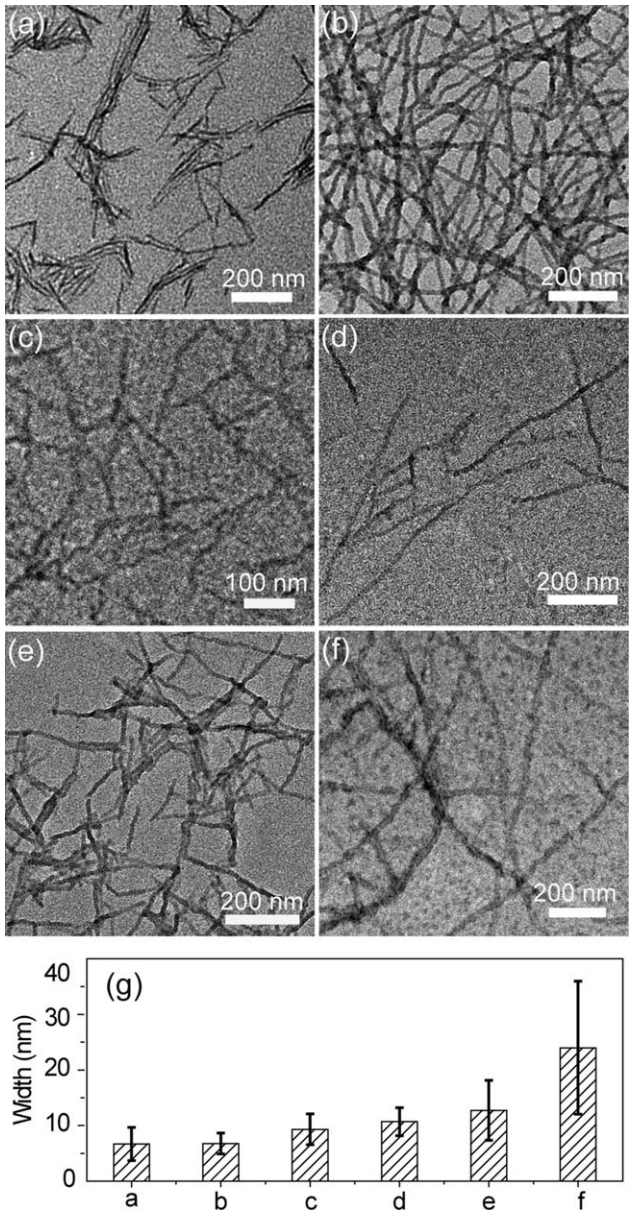

Figure 5. TEM images of cylindrical micelles obtained by assembly of P3HT-*b*-PEO in binary solvent mixtures: (a) *n*-hexane/THF, (b) methanol/toluene, (c) Et_2O/CS_2, (d) ethanol/xylene, (e) Et_2O/toluene, and (f) water/THF. (g) Relationship between diameters of the cylindrical micelles and different solvent mixtures.

the force balance contributing to the free energy of the system was affected, and the Flory–Huggins parameter (χ) of the mixed solvents increased gradually. These suggest that the incompatibility between the copolymer and mixed solvents raised, resulting in high degree of crystallization.[65] Initially, the polymer chains were completely dissolved in a good solvent. Addition of poor solvent lowered the solubility of P3HT in the mixed solution, and polymer chains begin to shrink and self-assemble into cylindrical micelles as the concentration of poor solvent increased. Yet, the formed cylindrical micelles may be disturbed, further aggregated, and finally precipitated out when the ratio of Et_2O/toluene beyond 4 : 1.

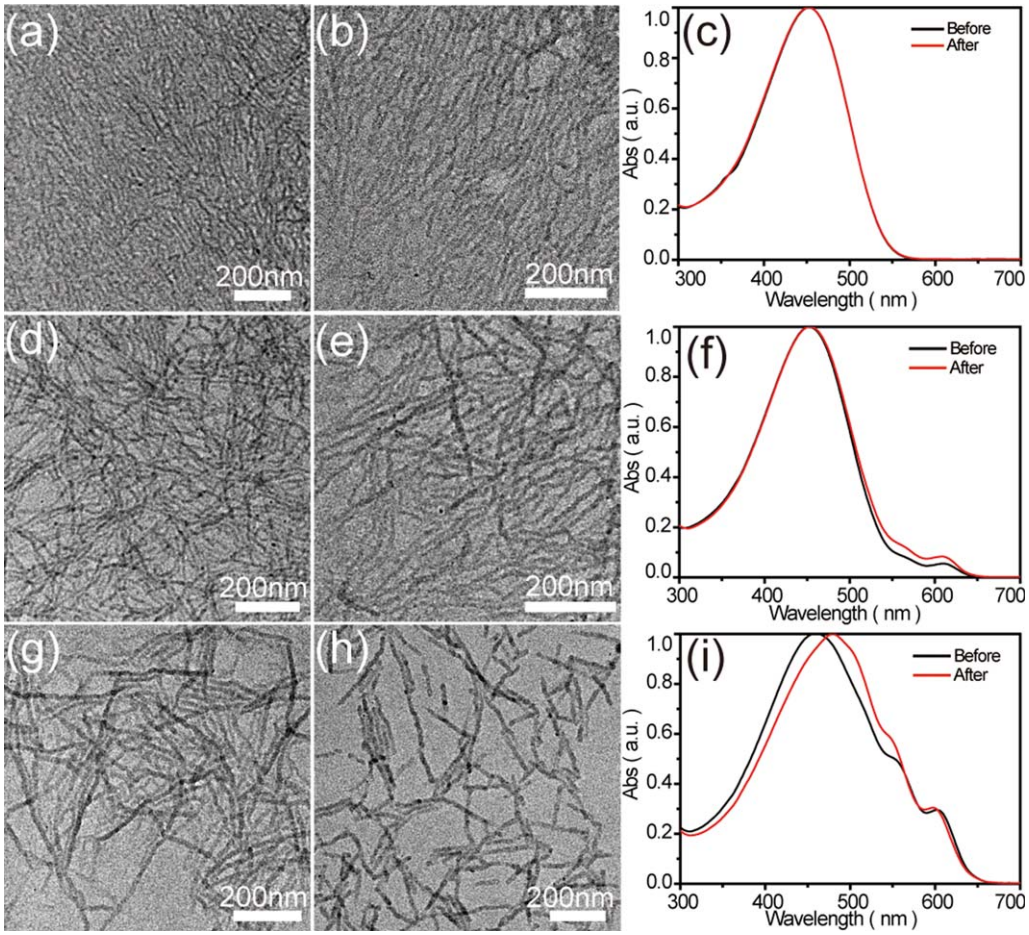

Figure 6. TEM images and corresponding UV–vis spectra before (a, d, g) and after (b, e, h) ultrasonic processing of the cylindrical micelles from assembly of P3HT-*b*-PEO in Et_2O/toluene with different ratio: (a–c) 1 : 5; (d–f) 1 : 2, and (g–i) 1 : 1. Clearly, there is a large change for the length of cylindrical micelles in 1 : 1, from greater than 1 μm (g) to about 200 nm (h). [Color figure can be viewed in the online issue, which is available at wileyonlinelibrary.com.]

Effect of Different Binary Solvents Mixtures on the Micellar Morphology

To further illustrate the generality of this approach, investigations were performed with different binary solvent mixtures. Varying solvent mixtures with different ratio, varied solubility χ of the copolymer in the solution can be achieved. Figure 5 shows the cylindrical micelles obtained from assembly of P3HT-*b*-PEO in disparate solution systems, including *n*-hexane/THF, methanol/toluene, Et_2O/CS_2, ethanol/xylene, Et_2O/toluene, and water/THF. A wide range of cylindrical micelles with varied widths can be obtained in these systems. This result implies that variation of solvent type and ratio can tune χ, and cylindrical micelles with certain width and length can thus be produced through adopting a desirable binary solvent mixtures.

Effect of Ultrasonic Processing on the Assembly Structures of P3HT-b-PEO

Furthermore, we employ ultrasonic processing to post-treat the formed cylindrical micelles obtained from different volume ratio of Et_2O/toluene systems. In this case, the working frequency of ultrasonication is kept at 40 KHz. P3HT-*b*-PEO solutions were oscillated for 10 min at temperature of 25°C with oscillating power of 100 %. Figure 6 reveals TEM images of the cylindrical micelles before and after ultrasonic processing. When small amount of Et_2O is added (e.g., Et_2O/toluene ratio = 1 : 5), ultrasonic treatment will not significantly vary the structure of the cylindrical micelles [Figure 6(a,b)]. The UV–vis spectra in Figure 6 offer additional information to support the above TEM investigation. Clearly, the curves are nearly coincident before and after sonication treatment when the ratio of poor/good solvent is 1 : 5. Yet, sonication processing will decrease the length of the cylindrical micelles when the amount of added Et_2O is large enough [see Figure 6(g,h)]. In the UV–vis spectra, in this case, the shoulder peaks present more intensive after being treated with ultrasonic. When Et_2O content (e.g., Et_2O/toluene = 1 : 1) was further increased, the absorption maximum peak at 450 nm is red-shifted while "shoulder" peaks at 550 and 600 nm are blue-shifted, which can be attributed to the increased planarity of the packed P3HT-*b*-PEO chains but a break of conjugation length.

During ultrasonic oscillating, the strong power facilitates polymer molecules to interact with solvent molecules intensely, leading to a decreased extension of chains entanglement. When the

polymer solution is dominated by the good solvent, the polymer chains have more freedom to relax into a more thermodynamically favorable conformation rather than being locked in an unfavorable conformation, thus the cylindrical micelles show no significant change even after the cylindrical micelles are broken by ultrasonic vibration. In this case, the ultrasonic processing contributes more to promote the disorder–order transformation in solution. When large amount of poor solvent is added, the polymer chains can be frozen and locked in an unfavorable conformation which cannot rearrange after breaking, and during this period the order–disorder transformation dominates.

CONCLUSIONS

In conclusion, we have synthesized the amphiphilic conjugated BCP, P3HT-*b*-PEO, and our results suggest that the addition of PEO block has no influence on the effective conjugation length of P3HT block. The presence of the PEO corona apparently provides colloidal stability and prevents the formation of the nanofibrillar aggregates characteristic of the P3HT homopolymer.[59] Introduction of poor solvent to good solvent containing P3HT-*b*-PEO will induce the crystallization-driven assembly of the P3HT into cylindrical micelles with a P3HT core, owing to π–π stacking of the conjugated backbone P3HT. The absorption spectra of the cylindrical micelles reveal a red shift as compared to the polymer in good solvent, indicating the extension of conjugation length with an improved π–π stacking of the polymer chains within the cylindrical micelles. Our results indicated that cylindrical micelles with varied diameter and length can be obtained by tuning the solvent properties. More interestingly, we demonstrate that ultrasonic processing can fragment the cylindrical micelles only when the ratio of poor solvent increases. The widths and lengths of the cylindrical micelles can be tuned using the disparate mixed solution and sonication processing, and this provides a facile and effective way to fabricate cylindrical micelles for applications in the area of polymer solar cell as well as organic optoelectronics device. This approach can also be applied to generate assemblies with well-defined structures for similar BCPs with core-forming π-conjugated blocks with different band gaps, which would be of considerable interest.

ACKNOWLEDGMENTS

We gratefully acknowledge funding for this work provided by the National Natural Science Foundation of China (91127046), Excellent Youth Foundation of Hubei Scientific Committee (2012FFA008), and Fundamental Research Funds for the Central Universities (HUST: 2013ZZGH016). We also thank the HUST Analytical and Testing Centre for allowing us to use its facilities.

REFERENCES

1. Günes, S.; Neugebauer, H.; Sariciftci, N. S. *Chem. Rev.* **2007**, *107*, 1324.
2. Jørgensen, M.; Norrman, K.; Gevorgyan, S. A.; Tromholt, T.; Andreasen, B.; Krebs, F. C. *Adv. Mater.* **2012**, *24*, 580.
3. Chen, J. W.; Cao, Y. *Acc. Chem. Res.* **2009**, *42*, 1709.
4. Chen, L.; Hong, Z.; Li, G.; Yang, Y. *Adv. Mater.* **2009**, *21*, 1434.
5. Thompson, B. C.; Frechet, J. *Angew. Chem. Int. Ed.* **2008**, *47*, 58.
6. Kim, Y.; Cook, S.; Tuladhar, S. M.; Choulis, S. A.; Nelson, J.; Durrant, J. R.; Bradley, D.; Giles, M.; Mcculloch, I.; Ha, C. S.; Ree, M. *Nat. Mater.* **2006**, *5*, 197.
7. Coakley, K. M.; McGehee, M. D. *Chem. Mater.* **2004**, *16*, 4533.
8. Blom, P.; Mihailetchi, V. D.; Koster, L.; Markov, D. E. *Adv. Mater.* **2007**, *19*, 1551.
9. Xin, H.; Kim, F. S.; Jenekhe, S. A. *J. Am. Chem. Soc.* **2008**, *130*, 5424.
10. Ren, G. Q.; Wu, P. T.; Jenekhe, S. A. *Chem. Mater.* **2010**, *22*, 2020.
11. Topham, P. D.; Parnell, A. J.; Hiorns, R. C. *J. Polym. Sci. Polym. Phys.* **2011**, *49*, 1131.
12. Han, M.; Kim, H.; Seo, H.; Ma, B.; Park, J. *Adv. Mater.* **2012**, *24*, 6311.
13. Wu, P. T.; Ren, G. Q.; Kim, F. S.; Li, C. X.; Mezzenga, R.; Jenekhe, S. A. *J. Polym. Sci. Polym. Chem.* **2010**, *48*, 614.
14. Sun, Z.; Xiao, K.; Keum, J. K.; Yu, X.; Hong, K.; Browning, J.; Ivanov, I. N.; Chen, J.; Alonzo, J.; Li, D.; Sumpter, B. G.; Payzant, E. A.; Rouleau, C. M.; Geohegan, D. B. *Adv. Mater.* **2011**, *23*, 5529.
15. Botiz, I.; Darling, S. B. *Macromolecules* **2009**, *42*, 8211.
16. Gu, Z.; Kanto, T.; Tsuchiya, K.; Shimomura, T.; Ogino, K. *J. Polym. Sci. Polym. Chem.* **2011**, *49*, 2645.
17. Yu, X.; Xiao, K.; Chen, J. H.; Lavrik, N. V.; Hong, K. L.; Sumpter, B. G.; Geohegan, D. B. *ACS Nano* **2011**, *5*, 3559.
18. Lin, J. C.; Lee, W. Y.; Wu, H. C.; Chou, C. C.; Chiu, Y. C.; Sun, Y. S.; Chen, W. C. *J. Mater. Chem.* **2012**, *22*, 14682.
19. Sauve, G.; McCullough, R. D. *Adv. Mater.* **2007**, *19*, 1822.
20. Veldman, D.; Ipek, O.; Meskers, S.; Sweelssen, J.; Koetse, M. M.; Veenstra, S. C.; Kroon, J. M.; vanBavel, S. S.; Loos, J.; Janssen, R. *J. Am. Chem. Soc.* **2008**, *130*, 7721.
21. Barrau, S.; Andersson V., Zhang, F. L.; Masich, S.; Bijleveld, J.; Andersson, M. R.; Inganas, O. *Macromolecules* **2009**, *42*, 4646.
22. Zhang, Y.; Tajima, K.; Hashimoto, K. *Macromolecules* **2009**, *42*, 7008.
23. Yang, X.; Loos, J.; Veenstra, S. C.; Verhees, W. J. H.; Wienk, M. M.; Kroon, J. M.; Michels, M. A. J.; Janssen, R. A. J. *Nano Lett.* **2005**, *5*, 579.
24. Lee, E.; Hammer, B.; Kim, J.; Page, Z.; Emrick, T.; Hayward, R. C. *J. Am. Chem. Soc.* **2011**, *133*, 10390.
25. Choi, S. Y.; Lee, J. U.; Lee, J. W.; Lee, S.; Song, Y. J.; Jo, W. H.; Kim, S. H. *Macromolecules* **2011**, *44*, 1771.
26. Kim, F. S.; Jenekhe, S. A. *Macromolecules* **2012**, *45*, 7514.
27. Kim, D. H.; Jang, Y.; Park, Y. D.; Cho, K. *J. Phys. Chem. B* **2006**, *110*, 15763.
28. Lee, Y. J.; Kim, S. H.; Yang, H.; Jang, M.; Hwang, S. S.; Lee, H. S.; Baek, K. Y. *J. Phys. Chem. C* **2011**, *115*, 4228.

29. Kim, D. H.; Park, Y. D.; Jang, Y.; Kim, S.; Cho, K. *Macromol. Rapid Commun.* **2005**, *26*, 834.
30. Salammal, S. T.; Mikayelyan, E.; Grigorian, S.; Pietsch, U.; Koenen, N.; Scherf, U.; Kayunkid, N.; Brinkmann, M. *Macromolecules* **2012**, *45*, 5575.
31. Seki, S.; Saeki, A.; Choi, W.; Maeyoshi, Y.; Omichi, M.; Asano, A.; Enomoto, K.; Vijayakumar, C.; Sugimoto, M.; Tsukuda, S.; Tanaka, S. *J. Phys. Chem. B* **2012**, *116*, 12857.
32. Laforgue, A.; Robitaille, L. *Synth. Met.* **2008**, *158*, 577.
33. Kuo, C. C.; Wang, C. T.; Chen, W. C. *Macromol. Symp.* **2009**, *279*, 41.
34. Kim, T.; Im, J. H.; Choi, H. S.; Yang, S. J.; Kim, S. W.; Park, C. R. *J. Mater. Chem.* **2011**, *21*, 14231.
35. Patra, S. K.; Ahmed, R.; Whittell, G. R.; Lunn, D. J.; Dunphy, E. L.; Winnik, M. A.; Manners, I. *J. Am. Chem. Soc.* **2011**, *133*, 8842.
36. Gilroy, J. B.; Lunn, D. J.; Patra, S. K.; Whittell, G. R.; Winnik, M. A.; Manners, I. *Macromolecules* **2012**, *45*, 5806.
37. Kamps, A. C.; Fryd, M.; Park, S. *ACS Nano* **2012**, *6*, 2844.
38. Hammer, B. A. G.; Bokel, F. A.; Hayward, R. C.; Emrick, T. *Chem. Mater.* **2011**, *23*, 4250.
39. Li, L. G.; Lu, G. H.; Yang, X. N. *J. Mater. Chem.* **2008**, *18*, 1984.
40. Berson, S.; De Bettignies, R.; Bailly, S.; Guillerez, S. *Adv. Funct. Mater.* **2007**, *17*, 1377.
41. Zhu, J. T.; Yu, H. Z.; Jiang, W. *Eur. Polym. J.* **2008**, *44*, 2275.
42. Zhu, J. T.; Zhao, J. C.; Liao, Y. G.; Jiang, W. *J. Polym. Sci. Polym. Phys.* **2005**, *43*, 2874.
43. Zhu, J. T.; Ferrer, N.; Hayward, R. C. *Soft Matter* **2009**, *5*, 2471.
44. Segalman, R. A.; McCulloch, B.; Kirmayer, S.; Urban, J. J. *Macromolecules* **2009**, *42*, 9205.
45. Yu, K.; Eisenberg, A. *Macromolecules* **1998**, *31*, 3509.
46. Bhargava, P.; Zheng, J. X.; Li, P.; Quirk, R. P.; Harris, F. W.; Cheng, S. Z. D. *Macromolecules* **2006**, *39*, 4880.
47. Sun, S. Y.; Salim, T.; Wong, L. H.; Foo, Y. L.; Boey, F.; Lam, Y. M. *J. Mater. Chem.* **2011**, *21*, 377.
48. Lee, J. Y.; Lin, C. J.; Lo, C. T.; Tsai, J. C.; Chen, W. C. *Macromolecules* **2013**, *46*, 3005.
49. Tu, G. L.; Li, H. B.; Forster, M.; Heiderhoff, R.; Balk, L. J.; Sigel, R.; Scherf, U. *Small* **2007**, *3*, 1001.
50. Leclere, P.; Hennebicq, E.; Calderone, A.; Brocorens, P.; Grimsdale, A. C.; Mullen, K.; Bredas, J. L.; Lazzaroni, R. *Prog. Polym. Sci.* **2003**, *28*, 55.
51. Jeffries-El, M.; Sauve, G.; McCullough, R. D. *Macromolecules* **2005**, *38*, 10346.
52. Jeffries-El, M.; Sauve, G.; McCullough, R. D. *Adv. Mater.* **2004**, *16*, 1017.
53. Loewe, R. S.; Ewbank, P. C.; Liu, J. S.; Zhai, L.; McCullough, R. D. *Macromolecules* **2001**, *34*, 4324.
54. Yamamoto, T.; Komarudin, D.; Arai, M.; Lee, B.; Suganuma, H.; Asakawa, N.; Inoue, Y.; Kubota, K.; Sasaki, S.; Fukuda, T.; Matsuda, H. *J. Am. Chem. Soc.* **1998**, *120*, 2047.
55. Chen, T.; Wu, X.; Rieke, R. D. *J. Am. Chem. Soc.* **1995**, *117*, 233.
56. Wu, P.; Ren, G.; Li, C.; Mezzenga, R.; Jenekhe, S. A. *Macromolecules* **2009**, *42*, 2317.
57. Xue, C. M.; Birel, O.; Xue, Y. H.; Dai, L. M.; Urbas, A.; Li, Q. *J. Phys. Chem. C* **2013**, *117*, 6752.
58. Xue, C. M.; Jin, S. *Chem. Mater.* **2011**, *23*, 2689.
59. Samitsu, S.; Shimomura, T.; Heike, S.; Hashizume, T.; Ito, K. *Macromolecules* **2008**, *41*, 8000.
60. Merlo, J. A.; Frisbie, C. D. *J. Phys. Chem. B* **2004**, *108*, 19169.
61. Ihn, K. J.; Moulton, J.; Smith, P. *J. Polym. Sci. Polym. Phys.* **1993**, *31*, 735.
62. Machui, F.; Abbott, S.; Waller, D.; Koppe, M.; Brabec, C. *J. Macromol. Chem. Phys.* **2011**, *212*, 2159.
63. Özdemir, C.; Güner, A. *Eur. Polym. J.* **2007**, *43*, 3068.
64. Eichinger, B. E.; Rigby, D. R., Stein, J. *Polymer* **2002**, *43*, 5999.
65. Park, Y. D.; Lee, H. S.; Choi, Y. J.; Kwak, D.; Cho, J. H.; Lee, S.; Cho, K. *Adv. Funct. Mater.* **2009**, *19*, 1200.